AJNR

Comparison of 2D and 3D Digital Subtraction Angiography in Evaluation of Intracranial Aneurysms

Takeshi Sugahara, Yukunori Korogi, Kouji Nakashima, Satoshi Hamatake, Shin Honda and Mutsumasa Takahashi

AJNR Am J Neuroradiol 2002, 23 (9) 1545-1552
http://www.ajnr.org/content/23/9/1545

AJNR Am J Neuroradiol 23:1545–1552, October 2002

Comparison of 2D and 3D Digital Subtraction Angiography in Evaluation of Intracranial Aneurysms

Takeshi Sugahara, Yukunori Korogi, Kouji Nakashima, Satoshi Hamatake, Shin Honda, and Mutsumasa Takahashi

BACKGROUND AND PURPOSE: **Although digital subtraction angiography (DSA) is considered the criterion standard for depiction of intracranial aneurysms, it is often difficult to determine the relationship of overlapping vessels to aneurysms when using 2D DSA. We compared 2D and 3D DSA in evaluation of intracranial aneurysms.**

METHODS: **Thirty-six consecutive patients with cerebral aneurysms underwent 2D and 3D DSA. After standard 2D DSA, rotational DSA was performed. Maximum intensity projection (MIP) and shaded surface display (SSD) images were created from the rotational DSA data sets. All images were assessed randomly for overall image quality, presence of aneurysm, presence of aneurysmal lobulation, visualization of aneurysmal neck, and relationship to adjacent vessels. Data analysis was conducted for 40 aneurysms treated by clip placement.**

RESULTS: **One aneurysm that was not detected at 2D DSA was classified as uncertain on the basis of rotational DSA. All aneurysms were classified as probably or definitively present on the basis of MIP and SSD findings. Overall image quality of rotational DSA, MIP, and SSD was statistically inferior to that of the standard 2D DSA for visualization of distal arteries. However, MIP and SSD images were significantly superior to those of standard 2D DSA for all other evaluations. For detection of lobulation, SSD images were significantly superior to other images, and for visualization of aneurysmal neck and relationship to neighboring arteries, SSD images were significantly superior to those of rotational DSA. For evaluation of the relationship to neighboring arteries, MIP images were significantly superior to those of rotational DSA.**

CONCLUSION: **Three-dimensional DSA, especially SSD, provided more detailed information for evaluating cerebral aneurysms than did standard 2D and rotational DSA.**

Determination of the size of an aneurysmal sac and neck and the anatomic relationship of an aneurysm to the vascular tree is essential for successful clip placement in the neck of a cerebral aneurysm and for interventional endovascular treatment. To obtain detailed morphologic information, digital subtraction angiography (DSA) has been considered to be the criterion standard because of excellent depiction of cerebrovascular anatomic structures with high image contrast and spatial resolution. However, it is often difficult to determine the relationship between multiple overlapping vessels from 2D projectional images. Furthermore, small vessels may be obscured when they are adjacent to large areas of opacification. When complex vascular structures are being imaged, it may be necessary to make multiple acquisitions at various angles to provide adequate visualization. However, multiple acquisitions result in increased radiation exposure to the patient and repeated injections of contrast material.

Recently, 3D DSA was introduced (1–3). With this technique, the 3D DSA images are reconstructed from a rotational 2D DSA data set. The reconstructed 3D DSA images show only the enhanced vascular lumina, and data are stored. Therefore, it is easy to evaluate the morphologic characteristics of an aneurysm from multiple views with the use of variable reconstruction techniques, such as multiplanar reconstruction, maximum intensity projection (MIP), shaded surface display (SSD), and volume rendering. Although some researchers have shown that 3D DSA is more sensitive for depiction of aneurysms than is 2D DSA, the number of patients and the detailed evaluation with a commercially available 3D DSA

Received May 31, 2001; accepted after revision April 30, 2002.

From the Departments of Radiology (T.S., K.N., S.Ha., S.Ho.), Health and Welfare Hospital, and the Kumamoto University School of Medicine (Y.K., M.T.), Kumamoto, Japan.

Address reprint requests to Takeshi Sugahara, MD, Department of Radiology, Kumamoto University School of Medicine, Honjo, Kumamoto, 860-8556, Japan.

system have been limited (1–3). Therefore, we obtained the standard 2D and 3D DSA images in patients with intracranial aneurysms and investigated the potential usefulness of 3D DSA compared with that of 2D DSA.

Methods

Patients

Between December 1999 and January 2001, 36 consecutive patients who were referred for evaluation of suspected intracranial aneurysms were prospectively examined. The patient group consisted of 11 (31%) male patients and 25 (69%) female patients ranging in age from 32 to 74 years (mean patient age, 61 years). At initial clinical presentation, 19 (53%) patients had subarachnoid hemorrhage (SAH) resulting from a ruptured aneurysm. Sixteen (44%) patients had no SAH but had MRA findings that were suspicious for aneurysms; in these 16, MRA had been performed for routine clinical examination or for ruling out vascular anomaly. One (3%) patient had progressive left third nerve palsy suggestive of an enlarging aneurysm of the left posterior communicating artery. Written informed consent for DSA examination was obtained from all patients.

Angiography

All patients underwent angiography while under local anesthesia. The device allowing 3D acquisition as well as 2D acquisition was a commercially available angiographic unit with a single X-ray tube and 9-inch image intensifier on a motorized C-arm (LCN+; GE Medical Systems, Buc, France). By using the Seldinger technique, the tip of a 5F catheter was guided from the femoral artery to the ascending aorta and positioned in the internal carotid or vertebral artery with the suspected intracranial aneurysm. Standard 2D DSA was initially performed to obtain anteroposterior and lateral views. X-ray parameters were 80 kV and 400 mA, a 1024 × 1024 matrix, and injection of 9 to 10 mL of contrast agent at a rate of 4 to 5 mL/s. Second, rotational angiography was performed by using the C-arm. This series rotated a total angular range of 220 degrees, but data acquisition was accomplished during the angular range of 200 degrees at 40 degrees/s, providing 44 projections with X-ray parameters of 80 kV and 250 mA and a 512 × 512 matrix. A total 15 mL of contrast agent was injected at a rate of 3 mL/s.

The method by which the rotational DSA produced the 3D angiograms was as follows. First, rotation of the C-arm was performed without injection to acquire the masks. Second, the C-arm rotated back to the initial position. Finally, the C-arm rotated again during injection of contrast material. The delay between the beginning of injection and acquisition of the first image was 1.2 to 1.5 seconds, determined as a reference of the standard 2D DSA. During image acquisition, real-time tasks, such as controlling C-arm movements, synchronizing X-ray exposures, and injecting contrast material, were handled automatically.

3D Reconstruction Techniques

The direct data obtained from the rotational DSA did not have the spatial accuracy necessary for the 3D reconstruction mainly because of two types of distortion: pincushion distortion and S distortion (1, 2, 4). Pincushion distortion results from the curvature of the input phosphor, and S distortion is caused by the effect of the surrounding magnetic fields on moving electrons within the image intensifier. Because the projection images were acquired at different image intensifier positions relative to the earth's magnetic field, the S distortion differed for each image. These image distortions were corrected by calculating the displacement for each pixel location at certain C-arm positioners and matching the acquired grid points to ideal grid points with the use of a grid phantom (4).

The acquisition geometry of the C-arm positions for each of the projection images was computed with the help of a calibration phantom called Helix, which consisted of a cylinder with markers arranged in a two and a half helical pattern. The C-arm geometry was calculated by modeling the imaging process as a transformation between the coordinate system defined by the X-ray source and the image intensifier and the coordinate system defined by the reference object. The transformation matrix relating a 3D point to its projection was decomposed into component matrices that described projection, rotation, and translation of the two coordinate systems relative to each other. The projection matrix is a function of the source to image distance and the image center. The three rotation matrices include the relative x-, y-, and z-axis angles. The translation matrix contains the location of the source with respect to the object center. The elements of the transformation matrix were estimated for each projection image, and the locations of the source and the image were determined with respect to the object coordinate system. Those calibrations were required every week.

Furthermore, to estimate gray levels of the retained voxels, an algebraic reconstruction method was used. With this reconstruction method, a set of ray equations is defined that equates each pixel gray value to the corresponding weighted sum of intercepted voxels. Starting from an initial estimate, one determines the voxel gray values through a series of iterative cycles. The method was generalized to 3D geometry determining the weighting parameters on the basis of the intersection volume between a ray and a voxel, adjusted for the voxel magnification.

After acquired data were corrected, the data were transferred to a workstation. It took approximately 7 minutes until the 3D data were available on the workstation. MIP, which was displayed with optimal windows, and SSD, which was displayed with optimal threshold, were reconstructed by a neuroradiologist (T.S.) who was experienced in cerebral angiography. Initially, MIP images, which were not required for any postprocessing, were displayed, and then SSD images were reconstructed. The optimal threshold of SSD images was appreciated as a reference of MIP images. Routinely, nine axial and nine coronal MIP images and nine axial and nine coronal SSD images were printed in sequential 10-degree rotation intervals. All 3D images were stereoscopically arranged. When the readers suspected aneurysms and required further information, they could independently examine the 3D images on the workstation from desired angles. Three-dimensional images were available approximately 10 to 15 minutes after 3D data were transferred to a workstation.

Image Analysis

Standard anteroposterior and lateral 2D DSA images and 18 rotational DSA images in sequential 13.6-degree rotational intervals were printed for evaluation. Films of all standard 2D DSA, rotational DSA, MIP, and SSD images were randomly arranged. Three readers (S.Ha, K.N.), who were unaware of clinical findings and did not take part in image manipulation, independently interpreted half of the films at separate sessions. Two months after the initial interpretation, three readers (S.Ha., K.N.) then independently evaluated the remaining films to minimize the risk of affecting the interpretation of one aspect of the study by others. After the independent review, a consensus reading was conducted to resolve any differences in interpretation. The readers evaluated all images randomly but could not be prevented from knowing which images were being reviewed, because the characteristic features of each image were easily identifiable. First, scoring of the overall image quality was performed on a four-point scale: 1 indicated that findings were inadequate for diagnosis; 2, findings made detection of an aneurysm possible but were not useful for diagnosis;

3, findings were good enough to detect an aneurysm, but visualization of cerebral arteries was not adequate; 4, findings were excellent for the diagnosis of an aneurysm, and visualization of cerebral arteries was adequate.

Scoring for the presence of an aneurysm was performed on a five-point scale: 1 was absent; 2, probably absent; 3, uncertain; 4, probably present; and 5, definitively present. If the answer was definitively present or probably present (score 4 or 5), the reader was then asked to evaluate the following characteristics of each aneurysm in question: presence of aneurysmal lobulation, visualization of aneurysmal neck, and separation of aneurysm from neighboring vessels. Scoring for presence of aneurysmal lobulation was performed on a five-point scale: 1 was absent; 2, probably absent; 3, uncertain; 4, probably present; and 5, definitively present. Scoring for visualization of aneurysmal neck and separation of aneurysm from neighboring vessels was performed on a four-point scale: 1 was poor; 2, fair; 3, good; and 4, excellent.

Data Analysis

Data analyses were conducted for the aneurysms verified with surgery. The analysis of variance and multiple comparisons were performed by using the Scheffé criterion (5) for each evaluation. $P < .01$ was considered statistically significant.

Results

Nine axial and nine coronal MIP images and nine axial and nine coronal SSD images provided a somewhat limited range of the potential views, but three readers thought that these images were enough for the evaluation of the presence of aneurysms. However, they sometimes needed observation of the images on the workstation to obtain different angles to get more detailed information on the characteristics of each aneurysm, such as the aneurysmal neck and the relationship of the aneurysm to surrounding vessels. One reader needed the workstation for seven patients to ensure the presence of aneurysm, one reader for 10 patients, and the other for 12 patients.

Forty-three aneurysms were detected and classified as probably or definitively present (grade 4 or 5) by all imaging techniques. Two untreated aneurysms and one treated aneurysm were undetected (grade 1), and one untreated aneurysm and one treated aneurysm were classified as uncertain (grade 3) on the basis of standard 2D DSA findings. One aneurysm that was undetected at standard 2D DSA was classified as uncertain and others were classified as probably or definitively present (grade 4 or 5) on the basis of rotational DSA results. All aneurysms were classified as probably or definitively present (grade 4 or 5) on the basis of MIP and SSD images. Finally, 48 aneurysms were detected. Data analysis was conducted for 40 aneurysms treated by clip placement. The locations of the evaluated aneurysms are detailed in Table 1.

Data for each evaluation are shown in Table 2. For overall image quality, the standard 2D DSA findings were superior those of other techniques ($P < .001$). The SSD images often did not show distal small cerebral arteries, and their scores were poorer than those of other images. Artifacts were present on rotational DSA images from misregistration between masks and images because of equipment vibration during the contrast agent injection, but they were minimal and did not degrade the MIP and SSD images (Figs 1 and 2). Motion artifacts, blurring of the vessel margin on the MIP images, and abnormal irregular structures on the SSD images were severe for only one patient (Fig 3).

TABLE 1: Location of aneurysms treated

Location	Aneurysms (n)
Anterior communicating artery	11
Posterior communicating artery	10
Middle cerebral artery	9
Posterior inferior cerebellar artery	3
Ophthalmic artery	2
Basilar artery	2
Internal cerebral artery	1
Anterior choroidal artery	1
Pericarosal artery	1
Total	40

For evaluation of the presence of an aneurysm, the MIP and SSD images were significantly superior to those of standard 2D DSA ($P < .001$), but no statistical difference was found between MIP and SSD images ($P = .547$) (Fig 1). The MIP and SSD images were superior to those of rotational DSA, although no statistical significance was found ($P = .422$ and .160, respectively).

For evaluation of the presence of lobulation, the SSD images were significantly superior to other images ($P < .001$). The SSD images clearly showed the lobulation from any angle, but other images did not always depict the lobulation, especially when the lobulation was overlaid on the aneurysm (Fig 2). The MIP images were also significantly superior to those of standard 2D DSA ($P = .006$), but no statistically significant difference between the rotational DSA and the MIP images was found ($P = .721$).

For visualization of aneurysmal neck and relationship to neighboring arteries, the MIP and SSD images were significantly superior to those of standard 2D DSA ($P < .001$), and the SSD images were significantly superior to those of rotational DSA ($P < .001$). The MIP and SSD images allowed the readers to view the images from the desired angles, and the most revealing images were easily identified (Figs 1 and 2).

Discussion

In the diagnostic workup of intracranial aneurysms, there are specific characteristics of the lesion and surrounding vessels that the radiologist must show, because many aneurysms that have been incompletely clipped have become enlarged or have rebled after surgical procedures (6, 7). Previous studies have documented that rupture of aneurysms was predictable after clip deployment because of the type and position of the aneurysm. For example, Drake et al (8) noted that in some instances, the clip had been placed across a lobulation instead of the neck. Sindou et al (7) showed that a large neck or large aneurysm most frequently had a remnant. Rauzzino et al (6) empha-

TABLE 2: The data of image analysis

	Presence of Aneurysm	Presence of Lobulation	Visualization of Aneurysmal Neck	Relationship to Neighboring Artery	Overall Image Quality
DSA	4.50 + 0.92	3.27 + 1.27	2.50 + 0.88	2.37 + 0.94	3.90 + 0.31†‡§
Rotation	4.83 + 0.45	3.83 + 1.23	3.60 + 0.65*	3.57 + 0.70*	3.56 + 0.54§
MIP	4.93 + 0.27*	3.94 + 1.08*	3.86 + 0.39*	3.86 + 0.43*†	3.44 + 0.54§
SSD	5.00 + 0.00*	4.54 + 0.99*†‡	4.00 + 0.00*†	4.00 + 0.00*†	3.06 + 0.25

Note.—DSA indicates digital subtraction angiography; MIP, maximum intensity projection; SSD, surface shaded display.

* Value is significantly greater than that of DSA.

† Value is significantly greater than that of rotational DSA.

‡ Value is significantly greater than that of MIP.

§ Value is significantly greater than that of SSD.

sized that incomplete visualization of an aneurysm because of its position in deep or beneath neighboring vessels or technical difficulty of clip deployment because of parent vessel perforators projecting near the aneurysm sac were important factors related to a poorer clip placement outcome.

Recently, methods of endovascular treatment have continued to evolve. The introduction of the Guglielmi detachable coil (9) allowed more controlled placement of coils and greater possibility of occlusion of the aneurysmal sac and neck. This technique is now becoming the treatment of choice in cases of surgically difficult or inoperable aneurysms (10–13). However, the success of embolization of an aneurysmal sac depends on many factors, such as the degree of the angle between the sac and parent artery, configuration of the aneurysmal sac, and differentiation of the neck from adjacent branches (13).

For the visualization of the aneurysmal neck and relationship to neighboring arteries, the MIP and SSD images were significantly superior to those of standard 2D DSA and rotational DSA. As noted, once an aneurysm is discovered, relevant geographic characteristics must be delineated, because the size of the neck relative to that of the aneurysm is one of the most important factors in endovascular planning (13). Additionally, knowledge of the neck site and surrounding vessels is inevitably needed for clip deployment, especially when exposure of the neck is insufficient. In addition, the 3D images could be easily positioned at the surgical view, which made it easier for neurosurgeons to clip the aneurysms.

For the presence of lobulation, the SSD images were significantly superior to those of MIP, standard 2D DSA, and rotational DSA. The morphologic characteristics of the aneurysm must be displayed, because this is a key feature of predicting ruptured aneurysms (12). Inherently, the SSD images can display the surface structure and provide a 3D vascular survey, and the readers can easily identify the aneurysmal surface and contour without having them obscured by overlying vessels, even in a single image. Although the SSD method is threshold-dependent with subsequent reduction of information and is judged unfavorably in comparison with the MIP method, the source images show only a vascular tree filled with contrast agent. Therefore, the density of enhanced vascular lumina is extremely higher than that of background or misregistration artifacts due to equipment vibration, and the reconstructed images were considered to be reliable.

The MIP and SSD images of 3D DSA were also significantly superior to those of standard 2D DSA and rotational DSA for evaluation of the presence of aneurysms. Improving the detection of aneurysms is very important, because approximately one fourth of patients with aneurysms have multiple aneurysms. Cases of undetected subarachnoid hemorrhage at angiography, even at standard 2D DSA, have been reported (9). In particular, when a subtle angiographic abnormality is encountered and other aneurysms are not detected on the angiograms, it is very difficult to decide whether surgical exploration should be performed. Three-dimensional DSA can more clearly depict the subtle angiographic abnormalities. To avoid unnecessary and costly surgery, we advocate the use of 3D DSA in the evaluation of cerebral aneurysms.

Although our results look promising, it is important to note that image quality is degraded by some artifacts. First, misregistration due to equipment vibration was always observed. These artifacts were often encountered at bony structures of the skull base. Fortunately, most cerebral aneurysms that required treatment were located near the circle of Willis, where the overlap of skull base bones was relatively minimal and the evaluation of cerebral aneurysms was not made difficult by the artifacts. Second, small vessels originating near the aneurysm and distal cerebral arteries might be obscured, because the injection volume of contrast agent per second is limited to decrease total volume and to avoid, as much as possible, adverse effects of contrast agent administration. In the present study, the injection rate for the 3D DSA was slower than that for the 2D DSA, although the total volume of contrast agent was larger for 3D DSA than for 2D DSA. The use of a slower injection rate for 3D DSA must have resulted in relatively poor visualization of distal cerebral arteries in comparison with standard 2D DSA. To determine the optimal volume of contrast agent, further investigation should be made in the future. Third, reconstructed images show only vascular lumina and may not allow differentiation of clotted blood from aneurysmal lumina. This information cannot be obtained with arterial angiography, and other imaging techniques such as

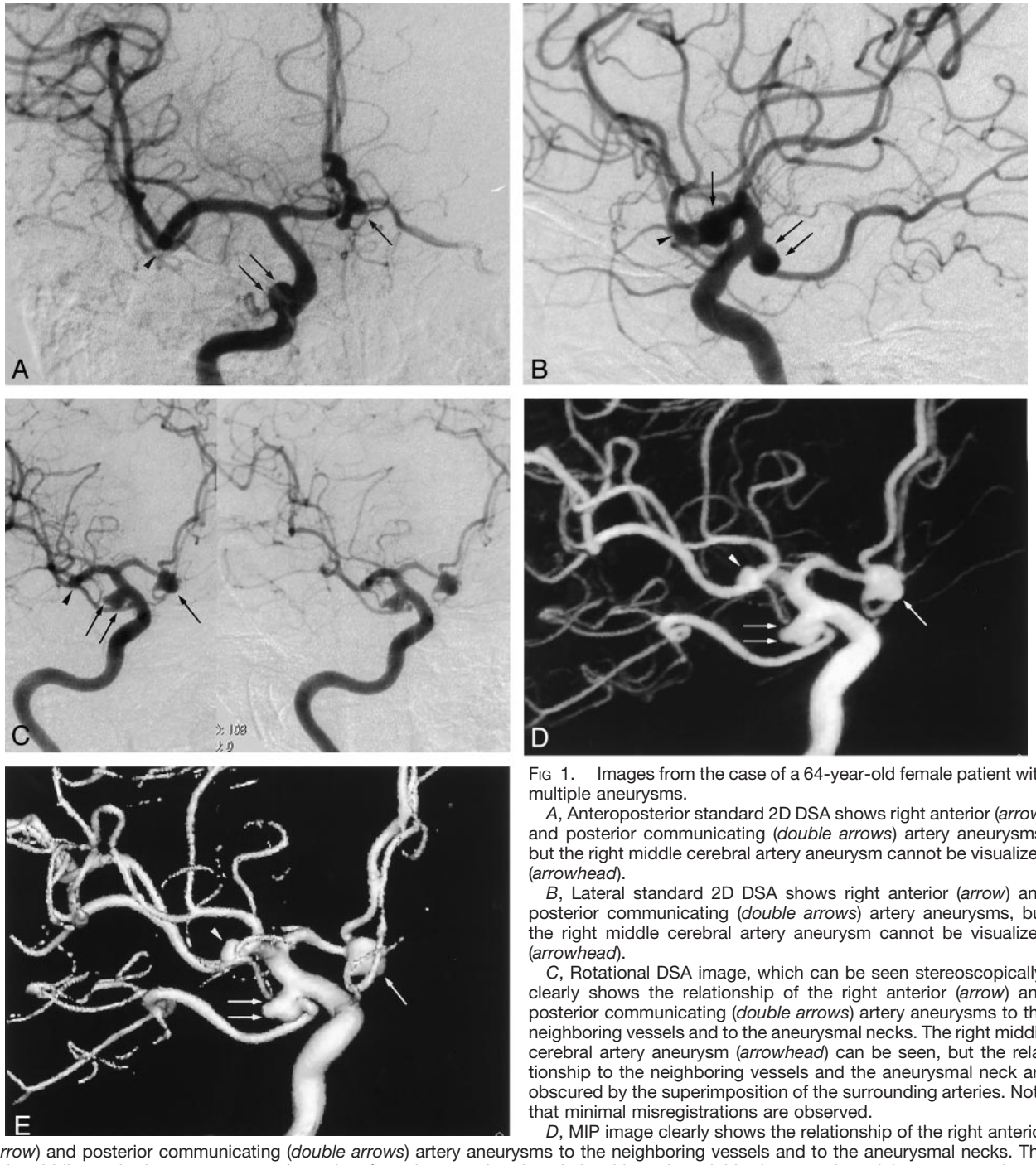

FIG 1. Images from the case of a 64-year-old female patient with multiple aneurysms.

A, Anteroposterior standard 2D DSA shows right anterior (*arrow*) and posterior communicating (*double arrows*) artery aneurysms, but the right middle cerebral artery aneurysm cannot be visualized (*arrowhead*).

B, Lateral standard 2D DSA shows right anterior (*arrow*) and posterior communicating (*double arrows*) artery aneurysms, but the right middle cerebral artery aneurysm cannot be visualized (*arrowhead*).

C, Rotational DSA image, which can be seen stereoscopically, clearly shows the relationship of the right anterior (*arrow*) and posterior communicating (*double arrows*) artery aneurysms to the neighboring vessels and to the aneurysmal necks. The right middle cerebral artery aneurysm (*arrowhead*) can be seen, but the relationship to the neighboring vessels and the aneurysmal neck are obscured by the superimposition of the surrounding arteries. Note that minimal misregistrations are observed.

D, MIP image clearly shows the relationship of the right anterior (*arrow*) and posterior communicating (*double arrows*) artery aneurysms to the neighboring vessels and to the aneurysmal necks. The right middle cerebral artery aneurysm (*arrowhead*) can be seen, but the relationship to the neighboring vessels and the aneurysmal neck are obscured by the superimposition of the surrounding arteries. Minimal misregistrations do not create artifacts.

E, SSD image clearly shows the relationship of the right anterior (*arrow*) and posterior communicating (*double arrows*) artery aneurysms to the neighboring vessels and to the aneurysmal necks. The right middle cerebral artery aneurysm (*arrowhead*) is seen, and the relationship to the neighboring vessels and aneurysmal neck are easily recognized. Minimal misregistrations do not create artifacts.

CT or MR imaging should be used. Fourth, the patient's motion artifacts produced more severe image degradation. Inherently, 3D DSA techniques required a longer acquisition time than did standard 2D DSA techniques and were more affected by the patient's motion. When a patient's motion is marked, we recommended repeating 3D DSA, or if impossible, conducting a detailed evaluation of the rotational and standard 2D DSA images. Finally, a relatively longer period (approximately 7 minutes) is required to produce 3D images. It is desirable to decrease postprocessing time, especially when interventional procedures are performed. This will be resolved with the development of computer hardware, but we thought that the time required to display 3D images was not so long as to prohibit routine use of this technique.

One limitation of this study was that only antero-

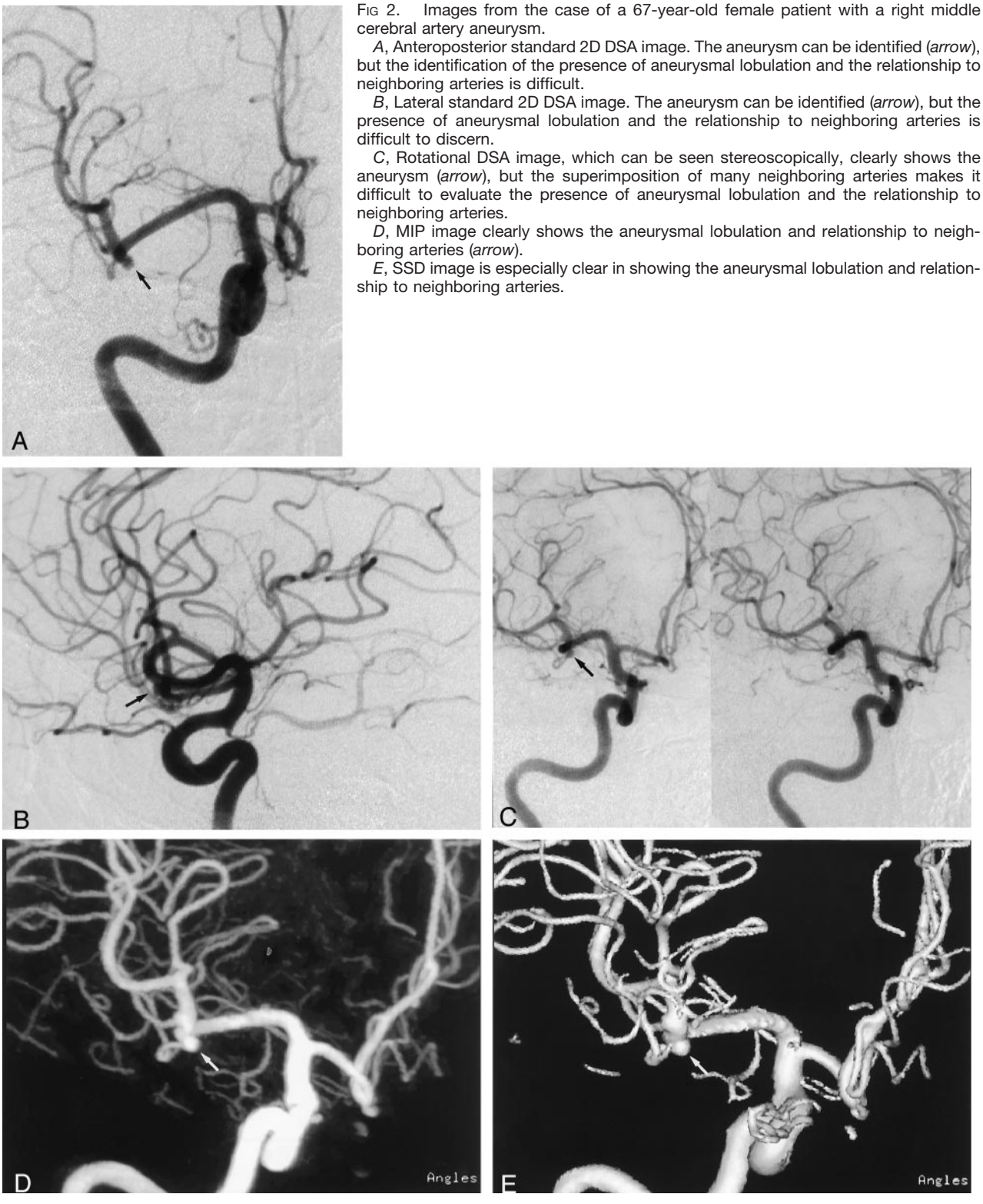

FIG 2. Images from the case of a 67-year-old female patient with a right middle cerebral artery aneurysm.

A, Anteroposterior standard 2D DSA image. The aneurysm can be identified (*arrow*), but the identification of the presence of aneurysmal lobulation and the relationship to neighboring arteries is difficult.

B, Lateral standard 2D DSA image. The aneurysm can be identified (*arrow*), but the presence of aneurysmal lobulation and the relationship to neighboring arteries is difficult to discern.

C, Rotational DSA image, which can be seen stereoscopically, clearly shows the aneurysm (*arrow*), but the superimposition of many neighboring arteries makes it difficult to evaluate the presence of aneurysmal lobulation and the relationship to neighboring arteries.

D, MIP image clearly shows the aneurysmal lobulation and relationship to neighboring arteries (*arrow*).

E, SSD image is especially clear in showing the aneurysmal lobulation and relationship to neighboring arteries.

posterior and lateral views were provided with standard 2D DSA. When an aneurysm is suspected on the basis of anteroposterior or lateral views, obtaining oblique images to adequately define the aneurysm anatomy would be warranted. A more appropriate study would be to obtain as many obliquities as are necessary to adequately define the aneurysm anatomy and then compare this with 3D DSA images. However, many oblique images would result in higher doses of contrast material, longer examination times, and more exposure to radiation. However, ethical and economic concerns may obviate such a comparison in a clinical study such as ours.

Recently, volume rendering, a third 3D technique

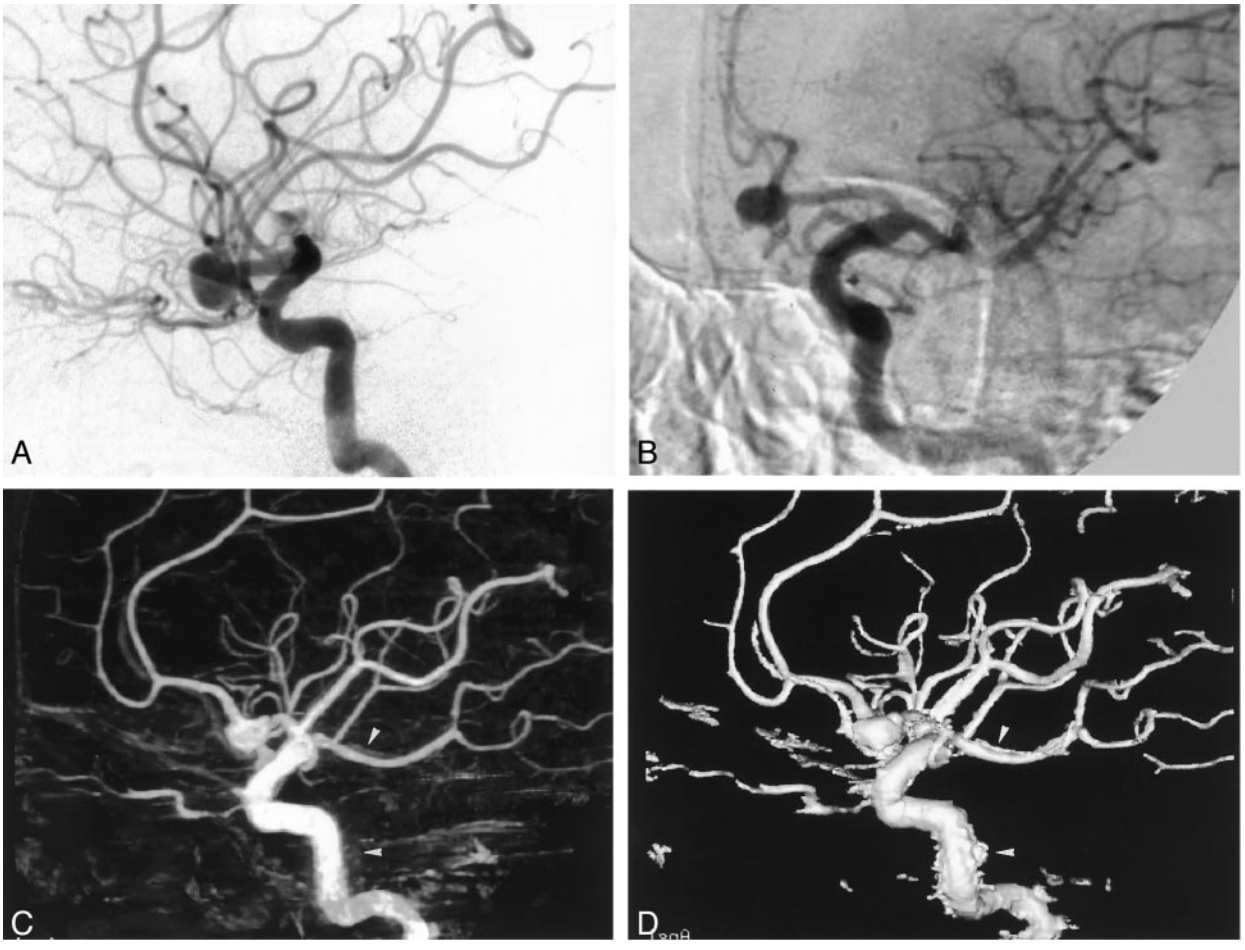

FIG 3. Images from the case of a 61-year-old male patient with a left anterior communicating artery aneurysm.
A, Lateral standard 2D DSA image. Few image artifacts are noted.
B, Rotational DSA image. Image artifacts are severe.
C, MIP image. Image artifacts create blurring (*arrowheads*).
D, SSD image. Image artifacts create abnormal irregular structures (*arrowheads*).

(14), has been introduced. This method has some advantages over the MIP and SSD techniques. First, the entire DSA data set can be incorporated within the 3D image, whereas a small fraction of data is displayed on MIP and SSD images. Second, the number, density, and opacity of voxels can be adjusted separately to allow a change in the transparency of selected materials. Finally, the 3D appearance is maintained and thereby enables a good analysis of the relationship among vascular structures. Although a longer period is required to reconstruct 3D images, because of the larger data set incorporated, more accurate evaluation is likely possible.

It should be possible to extend this technique to the evaluation of other vascular lesions, such as arteriovenous malformations, arterial stenosis, and vascular tumors, in various parts of the body. In addition, 3D DSA provides morphologic information. The information can be used for interventions such as percutaneous transluminal angioplasty and vascular stent placement.

Conclusion

Three-dimensional DSA, especially SSD images, clearly revealed aneurysms and aneurysmal lobulation, aneurysmal neck, and adjacent vessels without significant artifacts. Such detailed information is likely to be very useful for the surgical management, endovascular planning, and treatment of cerebral aneurysms.

References

1. Bidaut LM, Laurent C, Piotin M, et al. **Second-generation three-dimensional reconstruction for rotational three-dimensional angiography.** *Acad Radiol* 1998;5:836–849
2. Anxionnat R, Bracard S, Ducrocq X, et al. **Intracranial aneurysms: clinical value of 3D digital subtraction angiography in the therapeutic decision and endovascular treatment.** *Radiology* 2001;218:799–808
3. Heautot JF, Chabert E, Gandon Y, et al. **Analysis of cerebrovascular diseases by a new 3-dimensional computerised X-ray angiography system.** *Neuroradiology* 1998;40:203–209
4. Schueler BA, Sen A, Hsiung HH, Latchaw RE, Hu X. **Three-dimensional vascular reconstruction with a clinical X-ray angiography system.** *Acad Radiol* 1997;4:693–699
5. Fleiss JL. **The analysis of variance and multiple comparisons.** In:

The Design and Analysis of Clinical Experiments. New York: Wiley; 1986:51–59
6. Rauzzino MJ, Quinn CM, Fisher WS. **Angiography after aneurysm surgery: indications for "selective" angiography.** *Surg Neurol* 1998; 49:32–41
7. Sindou M, Acevedo JC, Turjman F. **Aneurysmal remnants after microsurgical clipping: classification and results from a prospective angiographic study (in a consecutive series of 305 operated intracranial aneurysms).** *Acta Neurochir (Wien)* 1998;140:1153–1159
8. Drake CG, Friedman AH, Peerless SJ. **Failed aneurysm surgery: reoperation in 115 cases.** *J Neurosurg* 1984;61:848–856
9. Guglielmi G, Viñuela F, Dion J, Duckwiler G. **Electrothrombosis of saccular aneurysms via endovascular approach: part 2. preliminary clinical experience.** *J Neurosurg* 1991;75:8–14
10. Nishioka H, Torner JC, Graf CJ, Kassell NF, Sahs AL, Goettler LC. **Cooperative study of intracranial aneurysms and subarachnoid hemorrhage: a long-term prognostic study: III. subarachnoid hemorrhage of undetermined etiology.** *Arch Neurol* 1984;41:1147–1151
11. Suzuki S, Kayama T, Sakurai Y, Ogawa A, Suzuki J. **Subarachnoid hemorrhage of unknown cause.** *Neurosurgery* 1987;21:310–313
12. Wood EH. **Angiographic identification of the ruptured lesion in patients with multiple cerebral aneurysms.** *J Neurosurg* 1964;21: 182–198
13. Cognard C, Weill A, Castaings L, Rey A, Moret J. **Intracranial berry aneurysms: angiographic and clinical results after endovascular treatment.** *Radiology* 1998;206:499–510
14. Ney DR, Fishman EK, Magid D, Robertson DD, Kawashima A. **Three-dimensional volumetric display of CT data: effect of scan parameters upon image quality.** *J Comput Assist Tomogr* 1991;15: 875–885